
Article:
Kepert, JD, Schwendike, J and Ramsay, H (2016) Why is the tropical cyclone boundary layer not "well-mixed"? Journal of the Atmospheric Sciences, 73 (3). pp. 957-973. ISSN: 0022-4928

https://doi.org/10.1175/JAS-D-15-0216.1

Why is the Tropical Cyclone Boundary Layer Not "Well Mixed"?

JEFFREY D. KEPERT

Research and Development Division, Bureau of Meteorology, Melbourne, Victoria, Australia

JULIANE SCHWENDIKE*

School of Earth, Atmosphere and Environment, Monash University, Clayton, Victoria, Australia

HAMISH RAMSAY

School of Earth, Atmosphere and Environment, and Australian Research Council Centre of Excellence for Climate System Science, Monash University, Clayton, Victoria, Australia

(Manuscript received 28 July 2015, in final form 14 October 2015)

ABSTRACT

Plausible diagnostics for the top of the tropical cyclone boundary layer include (i) the top of the layer of strong frictional inflow and (ii) the top of the "well mixed" layer, that is, the layer over which potential temperature θ is approximately constant. Observations show that these two candidate definitions give markedly different results in practice, with the inflow layer being roughly twice the depth of the layer of nearly constant θ. Here, the authors will present an analysis of the thermodynamics of the tropical cyclone boundary layer derived from an axisymmetric model. The authors show that the marked dry static stability in the upper part of the inflow layer is due largely to diabatic effects. The radial wind varies strongly with height and, therefore, so does radial advection of θ. This process also stabilizes the boundary layer but to a lesser degree than diabatic effects. The authors also show that this differential radial advection contributes to the observed superadiabatic layer adjacent to the ocean surface, where the vertical gradient of the radial wind is reversed, but that the main cause of this unstable layer is heating from turbulent dissipation. The top of the well-mixed layer is thus distinct from the top of the boundary layer in tropical cyclones. The top of the inflow layer is a better proxy for the top of the boundary layer but is not without limitations. These results may have implications for boundary layer parameterizations that diagnose the boundary layer depth from thermodynamic, or partly thermodynamic, criteria.

1. Introduction

The term "well mixed" is commonly used in meteorology to refer to boundary layers in which the potential temperature θ is nearly constant with height. This usage has presumably arisen because when an initially stably stratified layer is mixed by heating from the surface below, the result is a layer of approximately constant θ, surmounted by the original stable air. Mechanical stirring of the bottom of a stable layer in the absence of surface fluxes will produce a similar result. The term has some limitations, as mixing does not necessarily eliminate gradients. For example, if there is a source of a quantity at the bottom of the boundary layer and a sink at the top, then mixing within the layer will create a gradient across the layer, as commonly happens beneath land-based daytime subsidence inversions, where specific humidity decreases monotonically with height even though θ is nearly constant. Nevertheless, we will follow convention and take "well-mixed layer" as a synonym for the nearly constant-θ layer.

The popularity of the term partly reflects the fact that the well-mixed layer is often identical to the boundary layer. However, it is not the definition of the boundary layer, which is typically given as "The boundary layer is the lowest 1–2 km of the atmosphere, the region most

* Current affiliation: School of Earth and Environment, University of Leeds, Leeds, United Kingdom.

Corresponding author address: Jeffrey D. Kepert, Research and Development Division, Bureau of Meteorology, GPO Box 1289K, Melbourne VIC 3001, Australia.
E-mail: j.kepert@bom.gov.au

DOI: 10.1175/JAS-D-15-0216.1

directly influenced by the exchange of momentum, heat and water vapor at the earth's surface. Turbulent motions on time scales of an hour or less dominate the flow in this region, transporting atmospheric properties both horizontally and vertically throughout its depth'' (Kaimal and Finnigan 1994, p. v). This definition implies that we should look not just at θ in trying to define the boundary layer but at momentum and moisture also. It also implies that the turbulent fluxes are as important as the mean variables, if not more so, in determining where the top of the boundary layer lies. Since the turbulence transports heat, momentum, and moisture, there is often consistency between the boundary layer top derived from these three properties.

Observations of the tropical cyclone boundary layer therefore present a paradox. A composite analysis of a large number of dropsonde observations in the tropical cyclone core has shown that the inflow layer is about twice the depth of the well-mixed layer (Zhang et al. 2011). That is, defining the boundary layer depth from wind data yields very different results to using temperature data. The same phenomenon was noted earlier in the observational studies by Barnes and Powell (1995), Powell et al. (2003), Wroe and Barnes (2003), and Schneider and Barnes (2005), as well as in numerical simulations using WRF by Nolan et al. (2009a,b). The difficulty of defining the boundary layer top in tropical cyclones was also discussed by Smith and Montgomery (2010).

There is some evidence to suggest that the inflow layer is a better proxy than the well-mixed layer for the boundary layer in tropical cyclones. Measured vertical profiles of the momentum and moisture fluxes show that they approach zero not near the top of the well-mixed layer but near the top of the inflow layer (Zhang et al. 2009). Momentum budgets from a boundary layer model similarly show that the momentum flux magnitude becomes small near or slightly above the top of the inflow layer (Kepert 2010a,b, 2013). However, such data prompt the interesting question: why is the upper part of the inflow layer so stable? The wind shear in the tropical cyclone boundary layer is greater than almost anywhere else in the atmosphere, and anemometer time series attest to the intense turbulence thereby generated. Yet observations show that θ increases markedly with height in the upper half of the inflow layer. The reason cannot be that there is a source of θ at the top of the tropical cyclone boundary layer and a sink at the bottom, for observations of air–sea temperature differences (Cione et al. 2000) and the vertical θ structure (Zhang et al. 2011) imply that the heat flux is into the tropical cyclone boundary layer from both the top and bottom. What, then, maintains the marked θ gradient in the upper part of the inflow layer in the presence of such strong mixing?

In this article, we use the axisymmetric tropical cyclone model of Bryan and Rotunno (2009) to study the processes that determine the dry static stability $\partial\theta/\partial z$ in the lowest 1–2 km of a tropical cyclone. We describe the model setup in section 2. The modeled fields of heat and momentum are validated against Zhang et al.'s (2011) observations, and analyses of the budgets of θ and $\partial\theta/\partial z$ are given in section 3. Results are discussed in section 4 and conclusions summarized in section 5.

2. Model setup

Simulations were performed using the nonhydrostatic cloud model of Bryan and Fritsch (2002) (CM1; version 16), using the conservative equation set, in its axisymmetric configuration as described in Bryan and Rotunno (2009). The horizontal grid spacing is 2000 m everywhere, and the vertical grid is stretched, starting at 30 m and increasing gradually to a constant grid spacing of 500 m above 6.5 km. There are 12 model levels below 2 km. The domain extends radially out to 1500 km, and the model top is placed at 25 km. A Rayleigh damping zone is introduced in the uppermost 5 km to minimize reflectance of vertically propagating waves and also beyond 1400-km radius.

Sensible and latent heat fluxes are calculated using standard bulk aerodynamic formulas, with surface exchange coefficients for enthalpy C_k and momentum C_d fixed at 1.2×10^{-3} and 2.4×10^{-3}, respectively (i.e., $C_k/C_d = 0.5$). Turbulence is parameterized using a Smagorinsky-type scheme, in which the horizontal eddy viscosity depends on a prescribed horizontal length scale, chosen here to be 1000 m, while the vertical length scale is a function of height that tends toward ku_*z near the surface, where k is von Kármán's constant, u_* is the friction velocity, and z is height, and approaches 200 m as $z \to \infty$. Cloud microphysical processes are parameterized using the NASA Goddard version of the Lin–Farley–Orville (LFO) scheme. The Coriolis parameter is set at $5 \times 10^{-5}\,\mathrm{s}^{-1}$, and the sea surface temperature is fixed at 27°C. We present two simulations, with the sensible heating from turbulent dissipation (Bister and Emanuel 1998) either off or on. A broad, weak, vortex is introduced to the initial state, following Rotunno and Emanuel (1987), and initial temperature and moisture profiles are taken from the Atlantic hurricane season observations described in Dunion and Marron (2008).

Radiation is parameterized crudely by enforcing a fixed radiative cooling rate in the troposphere, while letting the stratospheric temperature relax back to a specified isothermal profile. When run for long enough,

this approach allows the system to reach a statistically steady state (e.g., Hakim 2011; Ramsay 2013; Chavas and Emanuel 2014) rather than be constrained by damping the temperature field back to a specified profile in both the troposphere and stratosphere, as is often done. The cooling rate is given by

$$\frac{\partial T}{\partial t} = \begin{cases} -1\,\mathrm{K\,d^{-1}} & \text{if} \quad T > T_{\mathrm{strat}} \\ (T_{\mathrm{strat}} - T)/(5\mathrm{d}) & \text{if} \quad T \le T_{\mathrm{strat}} \end{cases} \tag{1}$$

following Pauluis and Garner (2006), where T_{strat} is the specified stratospheric (isothermal) temperature, which is fixed at 196 K. A statistically steady storm structure is achieved after about 50 days of simulation (not shown). However, the model cyclone exhibits some significant fluctuations about that state in both the wind and thermodynamic structure. Accordingly, the results we present are for an average over days 50–120 of the simulation.

3. Results

a. Model validation

Figure 1 shows radius–height sections from the time-averaged model results, which can be compared to the composite analysis of Zhang et al. (2011) plotted in Fig. 2.[1] The mean RMW is near 40-km radius, with a peak azimuthal wind of 85 m s^{-1} at an altitude of 900 m. The inflow peak of 31 m s^{-1} is located at radius 50 km and altitude 100 m. Both these features are stronger than in the observed composite, which is expected because the composite includes storms of at least hurricane strength but not necessarily at maximum intensity, while the model simulation was spun up to its steady-state maximum intensity. The decay of the radial and azimuthal wind with radius is quicker in the model than in observations, and the inflow layer is deeper immediately outside of the RMW. This latter difference is qualitatively consistent with the more rapid decay in azimuthal wind, for that decay implies lower inertial stability outside of the RMW and, hence, a deeper boundary layer (Kepert 2001; Kepert and Wang 2001). The modeled θ structure shows a minimum at about 100-m height, similar to the observed composite, but the model values are generally a few degrees cooler. However, the model field is θ, while the observed field is virtual potential temperature θ_v, and if we instead compare model θ_v to observations (not shown), this difference nearly disappears. The modeled region of superadiabatic lapse rate (white to blue shading in Fig. 1e) is radially less extensive than in the observed composite but of similar depth. In both model and observations, the stability increases essentially monotonically with height at first, before becoming roughly constant with height. The height of the transition to roughly constant $\partial\theta/\partial z$ with height is a little higher in the model (around 1 km) than in the observations (around 700 m).

The model θ field shows a local minimum near the surface near 80-km radius, which is confined to the lowest few hundred meters. A similar weak minimum in θ is seen in the observational composite between 3 and 4 times the RMW and appears similar to the near-surface cooling noted by Cione et al. (2000) and Barnes and Bogner (2001) in this region. Another manifestation of this cooling is that the air–sea temperature difference increases inward toward the RMW (not shown), averaging about 1.3 K at 100-km radius and 3.3 K at 50 km, consistent with the observations reported by Cione et al. (2000) and Barnes and Bogner (2001).

For the model, the cloud frequency, defined as the proportion of output times for which each grid cell has cloud liquid water greater than 0.01 g kg^{-1}, is shown in Fig. 1f, along with the lifting condensation level (LCL) calculated from the model lowest-level fields. In and near the eye, the cloud base is around 100 m, increasing with radius. Outside the RMW, the lowest clouds observed are about 600 m, but the cloud base is more commonly near or slightly above 1 km, where it is cloudy $10^{-1/2} \approx 30\%$ of the time. This height corresponds with the level at which $\partial\theta/\partial z$ becomes roughly constant with height. The cloud base is only seldom as low as the surface LCL.

While there are some structural differences between model and observations, they are mostly connected with the model storm being more intense and having a steeper decay of azimuthal wind with radius. The overall stability structure is very similar, and therefore we suggest that the model simulation is sufficiently realistic that we can use it to study the processes that determine the stability structure in this part of the storm.

b. Thermodynamic budget

The budget equation for θ in CM1 is

$$\frac{\partial\theta}{\partial t} = -u\frac{\partial\theta}{\partial r} - w\frac{\partial\theta}{\partial z} - \Theta_1\theta\left(\frac{1}{r}\frac{\partial ru}{\partial r} + \frac{\partial w}{\partial z}\right) + \Theta_2\dot{q}_{\mathrm{cond}} + \Theta_3\varepsilon + D_{h,\theta} + D_{v,\theta} + N_\theta + R, \tag{2}$$

where we have followed Bryan and Rotunno's (2009) notation except that the diffusion term has been

[1] The data in Fig. 2 are from an updated version of Zhang et al.'s (2011) analysis, kindly provided by Jun Zhang, which incorporates additional observations but omits the spatial filtering.

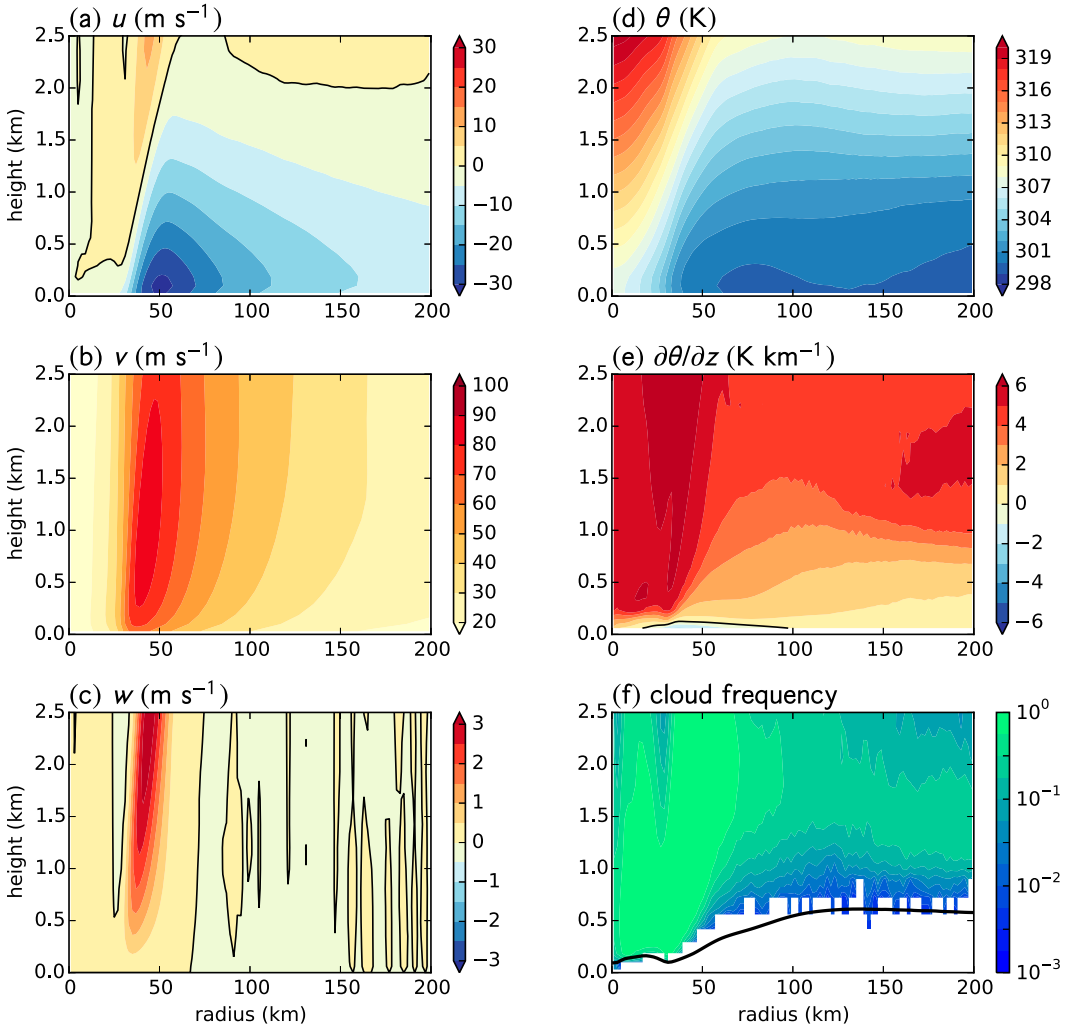

FIG. 1. Simulated mean boundary layer structure: (a) radial velocity (contour interval 5 m s^{-1}, zero contour in black), (b) azimuthal velocity (contour interval 10 m s^{-1}), (c) vertical velocity (contour interval 0.5 m s^{-1}), (d) potential temperature (contour interval 1 K), (e) stability (contour interval 1 K km^{-1}, zero contour in black), and (f) cloud frequency (contours in geometric progression starting at 10^{-3} and increasing by a factor of $10^{1/4}$), together with the surface LCL (black curve).

split into horizontal and vertical components, $D_\theta = D_{h,\theta} + D_{v,\theta}$. From left to right, these terms represent radial and vertical advection, the divergence term, latent heat exchange, heating due to viscous dissipation, horizontal and vertical diffusion, upper-level Newtonian damping, and radiative cooling. All budget terms are calculated from the 6-hourly model output data and then averaged from 50 to 120 days.

Figure 3 shows radius–height sections of the main terms in the θ budget, while Fig. 4 shows the same data averaged over annuli representing the eyewall (30–60 km) and outer radii (100–150 km). Note that the nonzero contours in Fig. 3 are spaced in geometric progression rather than linearly. The largest magnitudes in this budget occur in the eyewall, where the strong cooling tendency due to vertical advection nearly balances the diabatic warming above cloud base, as shown by the blue and black curves in Fig. 4a or by comparing Fig. 3c with Fig. 3e. Below cloud base in the eyewall, the diabatic heating term is negative, and this cooling together with significant cooling from radial advection is largely balanced by vertical diffusion—see the near-surface part of the black, red, and green curves in Fig. 4a, or compare Figs. 3a, 3c, and 3d. Horizontal diffusion and the divergence term are much smaller (Figs. 3b and 3f). At larger radii below about 1.1 km, the balance shifts to be largely between a warming tendency from vertical diffusion and a cooling tendency from the diabatic heating, with the sign of both terms changing above this height, as seen from the green and black curves in

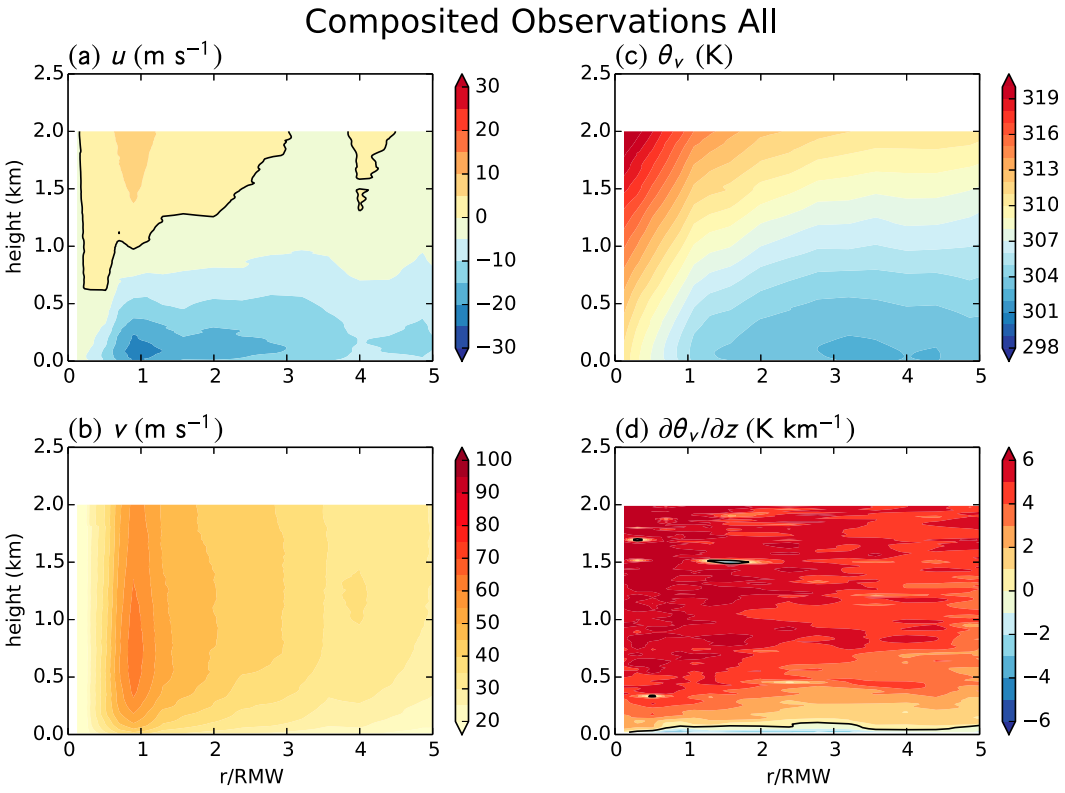

FIG. 2. Observed mean boundary layer structure. Data for all hurricanes from the updated dataset of Zhang et al. (2011): (a) radial velocity, (b) azimuthal velocity, (c) virtual potential temperature, and (d) stability. Contour intervals as in Fig. 1.

Figs. 4b and 4c. The zero contour of diabatic heating (Fig. 3e) corresponds reasonably well with the most frequent cloud base shown in Fig. 1f, consistent with the diabatic term representing rainfall evaporation below cloud base and condensational heating above. The horizontal advection (Fig. 3a) shows a relatively complex structure, with cooling through most of the region shown, owing to generally inward motion and a generally negative radial gradient of θ. Note that this cooling is not the same as the cooling due to adiabatic expansion, which is absent from this budget as we are considering θ. There are two significant exceptions to the general cooling: on the inner edge of the eyewall updraft where the outflow leads to a positive tendency and between about 80- and 115-km radius below 800-m height, where the radial θ gradient is reversed (Fig. 1d). This reversal of the radial gradient reflects the local minimum in θ near 80-km radius. That minimum coincides with the outer part of a broad maximum in diabatic cooling below 500 m (Fig. 3e), indicating that rainfall evaporation provides the cooling. At smaller radii, where the cooling is of similar strength, θ is warmer because the stronger heat-flux convergence, reflecting the greater surface heat flux, provides more rapid recovery (Fig. 3d). This difference is apparent in Fig. 4; while the mean near-surface diabatic heating (black) is quite similar in the 30–60- and 60–100-km annuli, the vertical diffusion term (green) is about twice as strong in the innermost annulus. That inward increase of the sensible heat flux convergence, not balanced by a similar increase in the diabatic cooling, defines the inner extent of the θ local minimum. Overall, the budgets nearly balance, as indicated by the thin black curves in Fig. 4.

It would be tempting to assume that the warming due to vertical diffusion reflects the fact that the sea surface is warmer than the overlying air, but the situation is more complex than that. The heat flux, shown in Fig. 3d by the yellow contours, is upward only immediately adjacent to the surface, and the heat flux in most of the region plotted is actually downward but decreasing in magnitude toward the surface. That is, the flux convergence that balances the evaporative cooling below 1 km is due more to mixing down from aloft than to the upward surface heat flux, as previously noted by Anthes and Chang (1978). The CBLAST heat flux observations (Zhang et al. 2009), although they are subject to a substantial

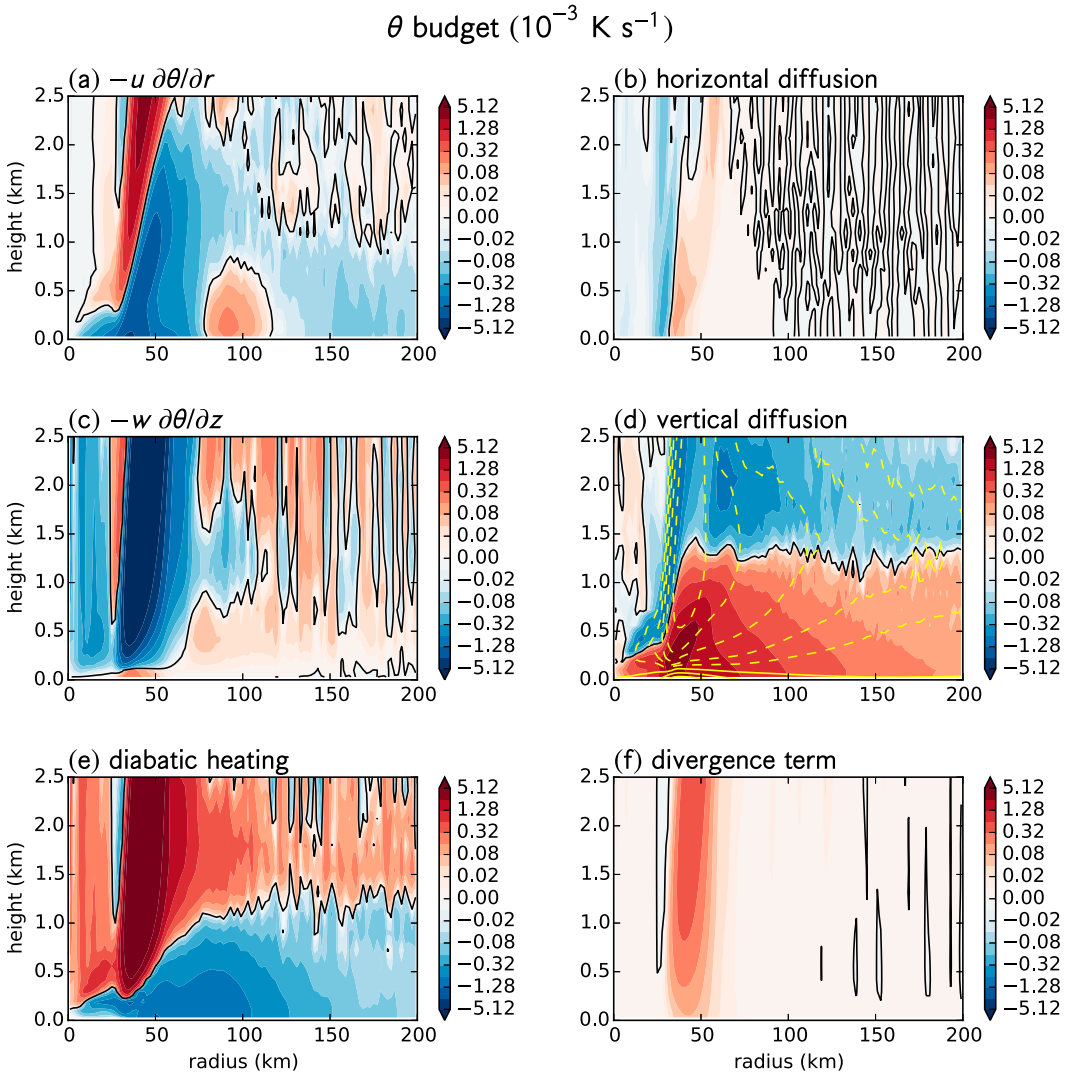

FIG. 3. Modeled θ budget for the run without dissipative heating: (a) radial advection, (b) horizontal diffusion, (c) vertical advection, (d) vertical diffusion, (e) diabatic heating, and (f) the divergence term. Contours in all panels are (apart from zero) in geometric progression, at $\{0, \pm1, \pm2, \pm4, \ldots, \pm512\} \times 10^{-5}\,\mathrm{K\,s^{-1}}$. Additionally included in (d) is the vertical heat flux in yellow contours, similarly spaced at $\{0, \pm1, \pm2, \pm4, \pm8, \pm16\} \times 10^{-1}\,\mathrm{K\,m^{-1}\,s^{-1}}$, with negative contours dashed.

amount of sampling error, tend to suggest a similar structure, albeit with the level of zero flux being located farther from the surface. These differences may be because those observations were taken at larger radius than shown here, and between rainbands, and may therefore reflect a boundary layer with less direct influence from cloud and rain processes than that examined here.

c. *The budget of* $\partial\theta/\partial z$

The budget equation for the stability $\partial\theta/\partial z$ was obtained by differentiating the θ budget in (2) with respect to z and rearranging

$$\frac{\partial}{\partial t}\frac{\partial\theta}{\partial z} = -u\frac{\partial}{\partial r}\frac{\partial\theta}{\partial z} - w\frac{\partial^2\theta}{\partial z^2} - \frac{\partial u}{\partial z}\frac{\partial\theta}{\partial r} - \frac{\partial w}{\partial z}\frac{\partial\theta}{\partial z} - \frac{\partial}{\partial z}\left[\Theta_1\theta\left(\frac{1}{r}\frac{\partial ru}{\partial r} + \frac{\partial w}{\partial z}\right)\right] + \frac{\partial\Theta_2\dot{q}_{\mathrm{cond}}}{\partial z} + \frac{\partial\Theta_3\varepsilon}{\partial z} + \frac{\partial D_{h,\theta}}{\partial z} + \frac{\partial D_{v,\theta}}{\partial z} + \frac{\partial N_\theta}{\partial z} + \frac{\partial R}{\partial z}. \quad (3)$$

The physical interpretation of the terms on the RHS is as follows.

- $-(u\,\partial/\partial r)(\partial\theta/\partial z)$ and $-w\partial^2\theta/\partial z^2$: Radial and vertical advection of stability, respectively.

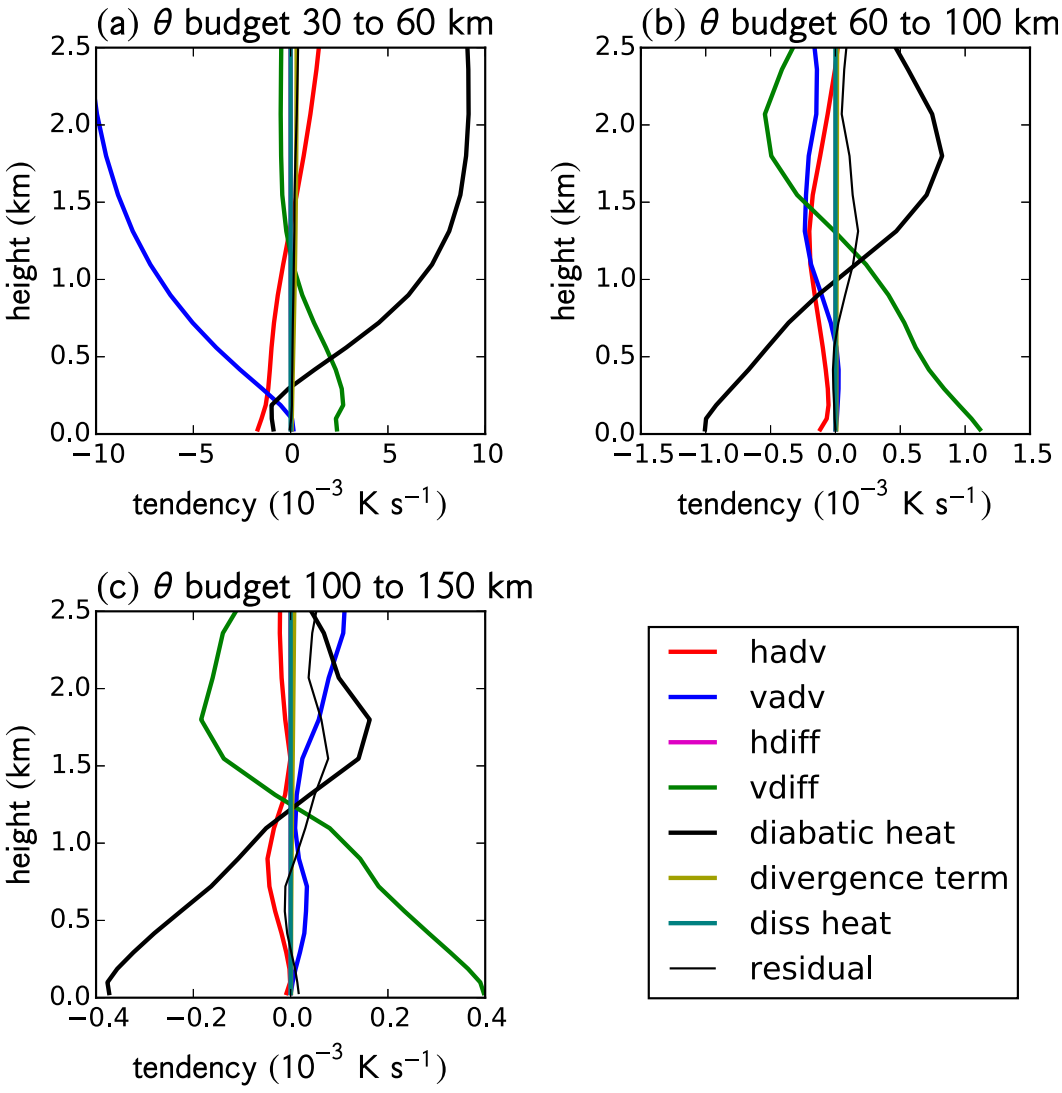

FIG. 4. Modeled θ budget for the run without dissipative heating, averaged over (a) 30–60, (b) 60–100, and (c) 100–150 km. Note the different scales on the abscissas.

- $-(\partial u/\partial z)(\partial\theta/\partial r)$: Differential horizontal advection, which occurs when u varies with height in the presence of a horizontal θ gradient. This process changes the magnitude of $\partial\theta/\partial r$ by tilting the isentropes to be more or less vertical. If they tip over, the sign of the stability changes.
- $-(\partial w/\partial z)(\partial\theta/\partial z)$: For stretching ($\partial w/\partial z > 0$), initially sloping isentropes will become more vertical and the stability moves toward zero, while the opposite applies for squashing ($\partial w/\partial z < 0$). The stability can change magnitude but not sign through this term.
- $(\partial/\partial z)\{\Theta_1\theta[(1/r)(\partial ru/\partial r) + (\partial w/\partial z)]\}$: Vertical derivative of the divergence term.
- $(\partial/\partial z)(\Theta_3\varepsilon)$: Vertical derivative of heating from turbulent dissipation.
- $(\partial/\partial z)(\Theta_2\dot{q}_{\rm cond})$: Diabatic heating through condensation and evaporation. Vertically varying diabatic heating will change the stability.
- $\partial D_{h,\theta}/\partial z$: Horizontal diffusion, which will tend to reduce horizontal gradients of stability.
- $\partial D_{v,\theta}/\partial z$: Vertical diffusion. Vertical mixing will normally tend to reduce $|\partial\theta/\partial z|$ because mixing tends toward constant θ. But it may also increase the gradient—for example, in situations where there are strong interfacial fluxes.
- $\partial N_\theta/\partial z$ and $\partial R/\partial z$: Vertical derivatives of Newtonian relaxation and radiative cooling, respectively. Both derivatives are zero in the troposphere.

Radius–height sections of the main terms in the $\partial\theta/\partial z$ budget are shown in Fig. 5, in which, red (blue) shading

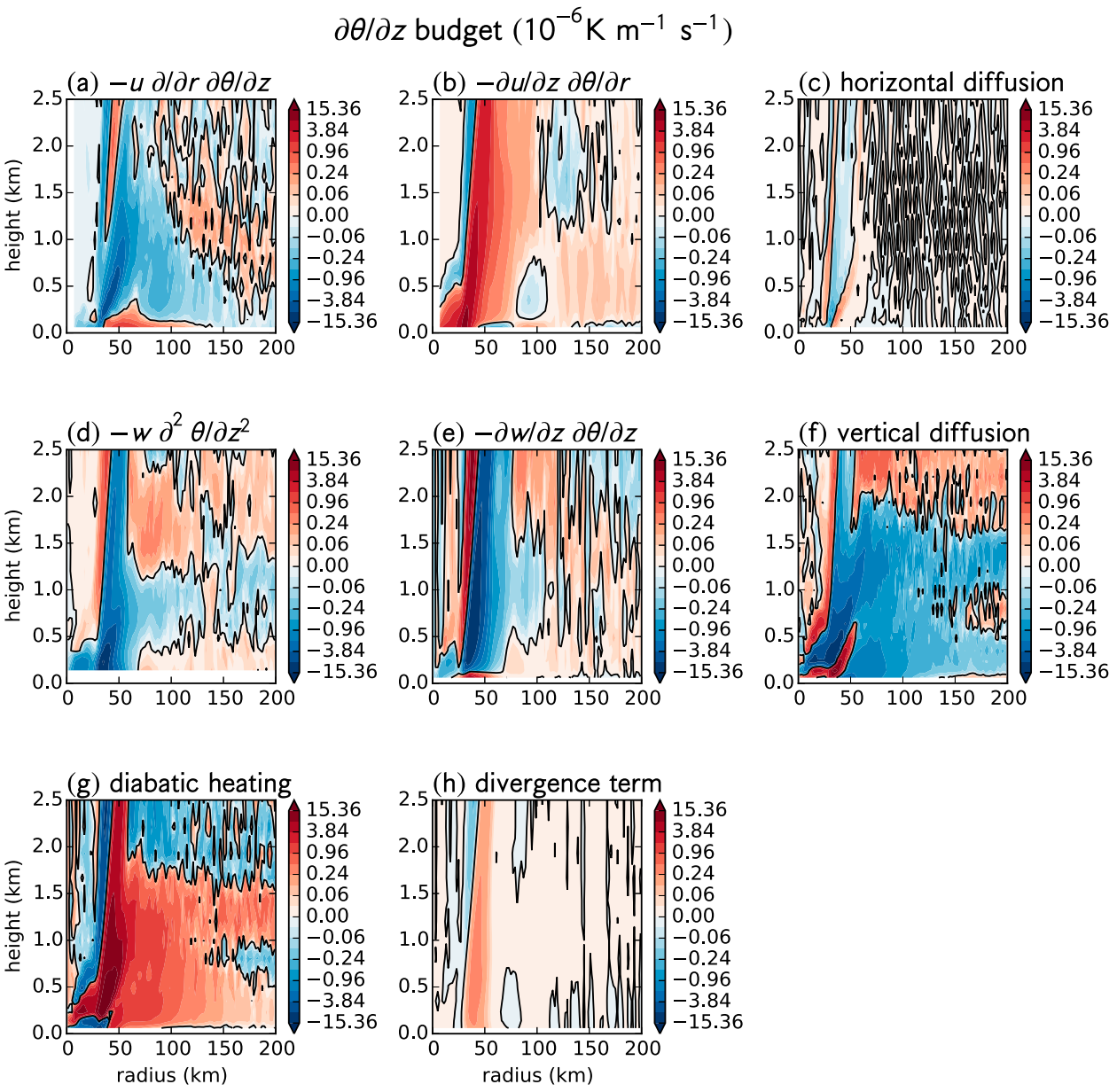

FIG. 5. Modeled $\partial\theta/\partial z$ budget for the run without dissipative heating: (a) radial advection, (b) differential radial advection, (c) horizontal diffusion, (d) vertical advection, (e) stretching, (f) vertical diffusion, (g) diabatic heating, and (h) the divergence term. Contours in all panels are in geometric progression, except for the zero contour, at values $\{0, \pm1, \pm2, \pm4, \ldots, \pm512\} \times 3 \times 10^{-8}$ K m^{-1} s^{-1}.

indicates that the process increases (decreases) the stability. Profile plots of the mean budget over the same annuli as before are in Fig. 6. In the vicinity of the eyewall (Fig. 6a), the budget term that makes the strongest contribution to stabilization is the diabatic term (Fig. 5g), with differential horizontal advection (Fig. 5b) and vertical diffusion near the surface (Fig. 5f) also making nonnegligible contributions. These are balanced by several terms: radial and vertical advection (Figs. 5a,d), vertical stretching (Fig. 5e), and, except near the surface, vertical diffusion (Fig. 5f). The horizontal diffusion and divergence term contributions are smaller (Figs. 5c,h).

At larger radii (Figs. 6b,c), the budget is dominated by the stabilizing effect of diabatic heating, roughly balanced by the destabilizing effect of vertical diffusion. Radial advection of stability is destabilizing below about 1 km, and stabilizing aloft, but of smaller magnitude. Differential radial advection is predominantly stabilizing, except near the surface and in the region of reversed radial θ gradient between about 80- and 120-km radius

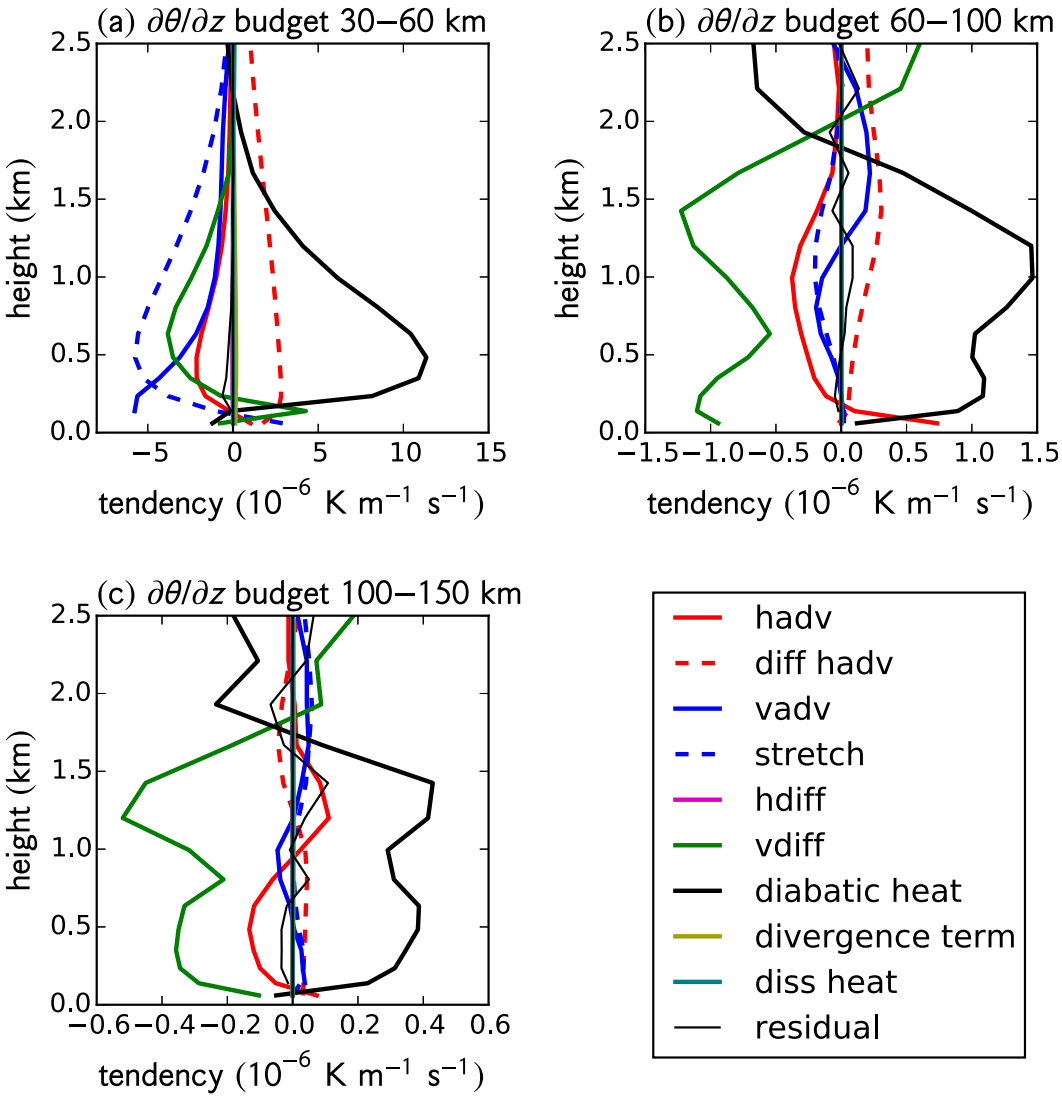

FIG. 6. Modeled $\partial\theta/\partial z$ budget for the run without dissipative heating, averaged over (a) 30–60, (b) 60–100, and (c) 100–150 km.

and from about 150- to 800-m height (Fig. 1d). The differential horizontal advection term also has regions of reversed sign below about 150-m height because the mean inflow there is increasing with height, so the vertical shear is tending to tilt the isentropes in the opposite sense to farther aloft.

The production of dry static stability in these budgets is dominated by diabatic heating, that is, by latent heat release above cloud base and rainfall evaporation below. In the vicinity of the eyewall, differential horizontal advection also contributes to the stabilization. Some caution is appropriate in drawing conclusions about causal relationships from budgets—for example, large terms in near balance may reflect competing physical processes or may simply reflect the way the equations have been structured (e.g., Tory et al. 2012). It is also important to ensure that the budgets nearly balance, as they do here. However, in this case vertical turbulent transport, differential horizontal advection, and diabatic heating are clearly independent processes and so we can conclude that the main reason that the inflow layer in a tropical cyclone has such marked dry static stability is diabatic processes, with a secondary contribution from differential horizontal advection.

d. The effect of heating from turbulent dissipation

The above analysis does not provide much insight as to the cause of the surface superadiabatic layer in Zhang et al.'s (2011) composite analysis, and indeed that simulation produced a much weaker and less extensive

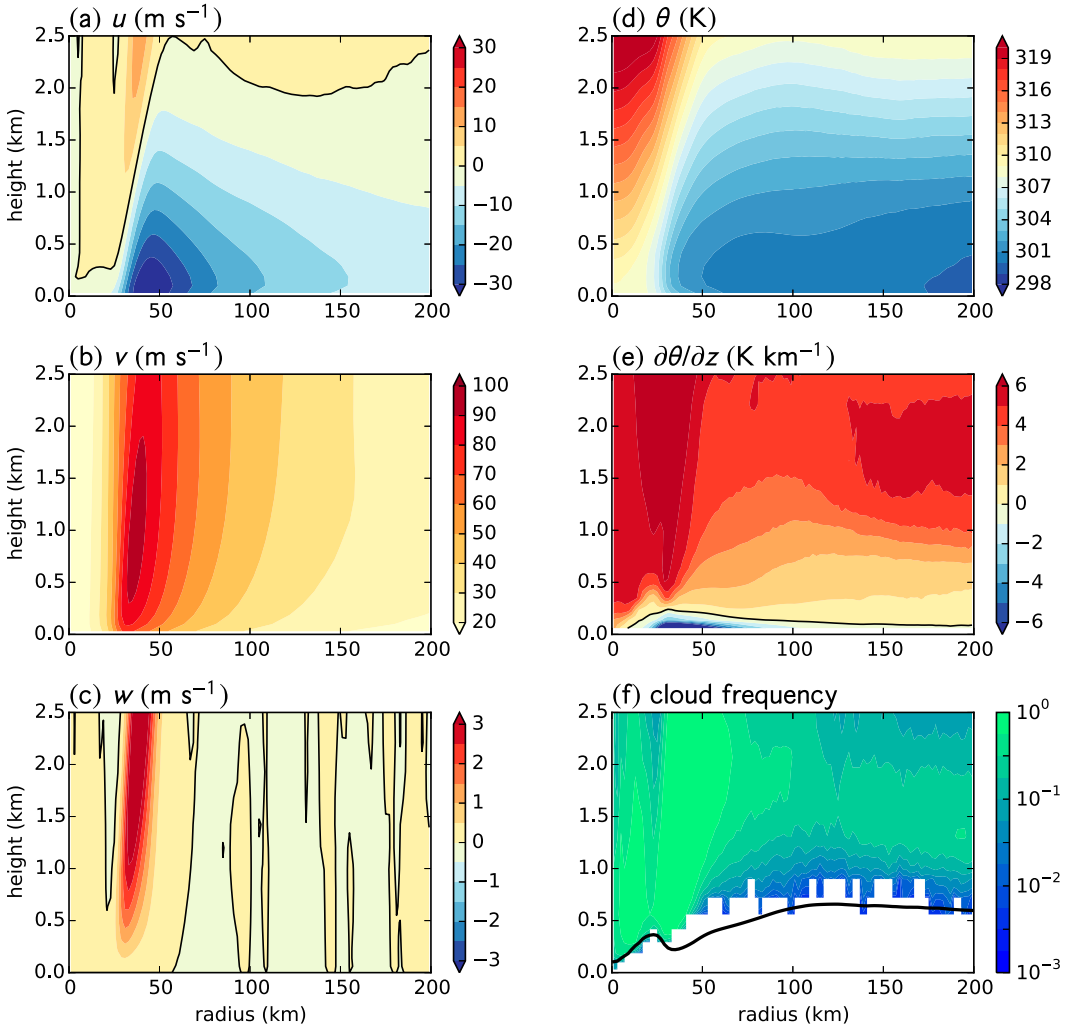

FIG. 7. As for Fig. 1, but for the run with dissipative heating on.

near-surface superadiabatic layer than observed. Heating due to turbulence dissipation depends on the dissipation rate, so it would be expected to be strongest near the surface. In principle, therefore, it has the right sign to contribute to near-surface destabilization. We now examine a simulation with this process included to determine the magnitude of its effect.

The cyclone structure is shown in Fig. 7. The azimuthal winds have increased compared to the previous run, qualitatively consistent with potential intensity theory (Bister and Emanuel 1998), with concomitant increases in the secondary circulation, but there are only small changes to the cloud-base statistics. Near-surface conditions are slightly warmer than before, and the surface superadiabatic region now extends out to in excess of 200-km radius and is much stronger near the RMW. The minimum in $\partial\theta/\partial z$ is now $-13.1\,\mathrm{K\,km^{-1}}$ rather than $-2.2\,\mathrm{K\,km^{-1}}$ in the previous simulation, compared to the strong near-surface gradients of about -6.8 and $-5.8\,\mathrm{K\,km^{-1}}$ in Zhang et al.'s (2011) updated composites of category 4 and 5 and all hurricanes, respectively. The superadiabatic layer also increases in strength and depth toward the RMW, consistent with Barnes's (2008) comment that "many of the soundings that manifest a superadiabatic lapse rate are near or under the eyewall" (p. 639). Although the near-surface superadiabatic layer is now stronger than observed, we note that the modeled cyclone is more intense and therefore has greater dissipative heating.

The θ budget (Fig. 8) is similar to before, except very near the surface where dissipative heating provides a strong positive tendency (Fig. 8g). Warming from this process also extends upward into the eyewall region but is small compared to other terms in that region. The strong near-surface warming from turbulent dissipation is largely balanced by changes to the vertical diffusion

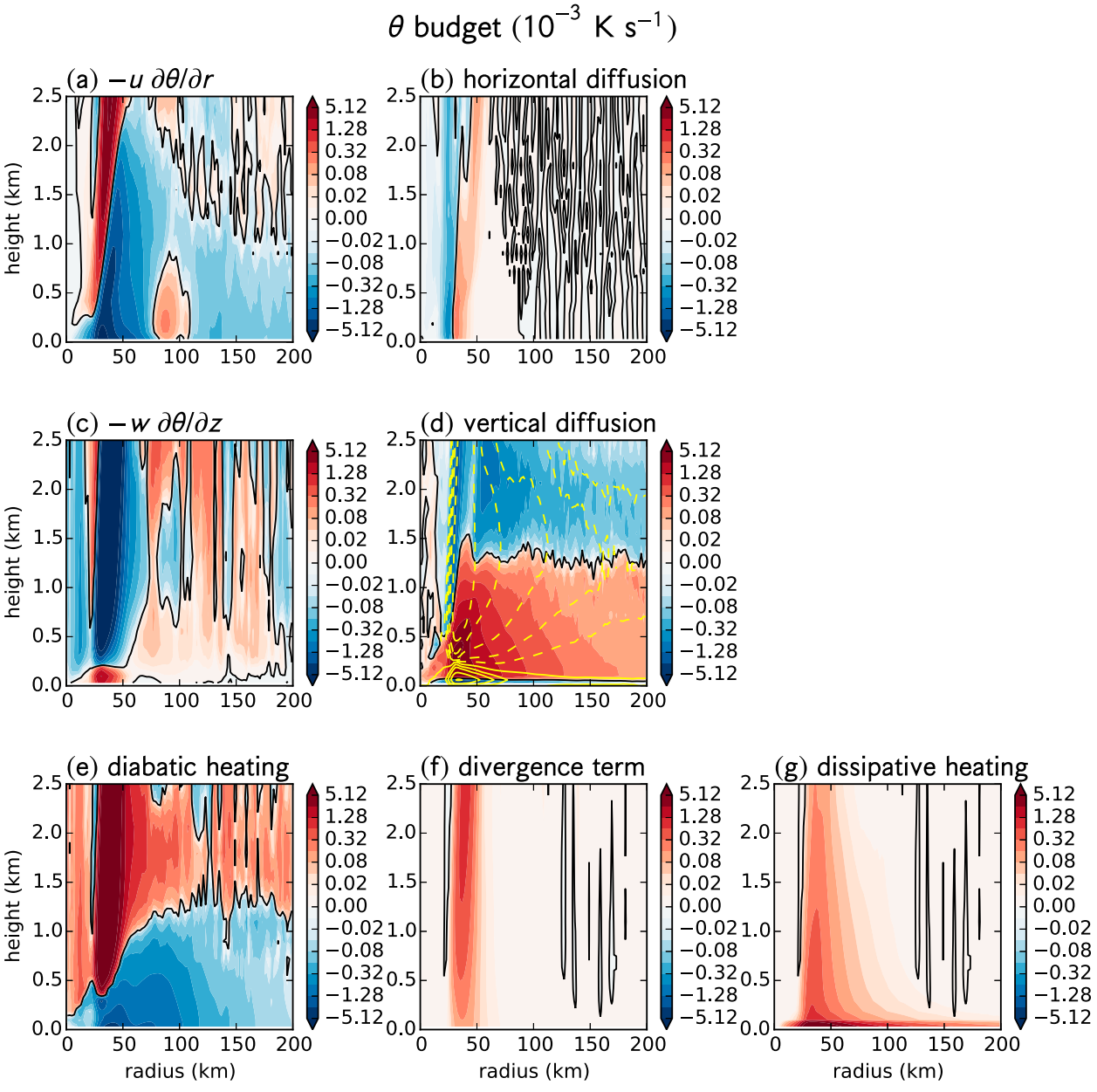

FIG. 8. As for Fig. 3, but for the run with dissipative heating on. (g) The dissipative heating rate.

(Fig. 8d), which now exhibits a strong cooling near the surface. That is, the turbulence transports the additional heat upward and away from its main source region.

The main changes to the dry static stability budget (Fig. 9) are also near the surface, where a strong destabilizing tendency from dissipative heating (Fig. 9i) is countered by vertical diffusion (Fig. 9f).

These results from the budget, together with the fact that the run with dissipative heating better matches the observed surface superadiabat in magnitude and radial extent, suggest that the main cause of this feature is heating from turbulent dissipation. Barnes (2008) identified dissipative heating as a possible cause for the observed near-surface superadiabatic layer and demonstrated that the strength of the superadiabat increased with wind speed, but he did not present a budget analysis. Our results confirm his suggestion and demonstrate that dissipative heating is intense enough to markedly affect the atmospheric temperature structure.

4. Discussion

From our budget analysis, the marked dry static stability in the upper part of the tropical cyclone inflow layer

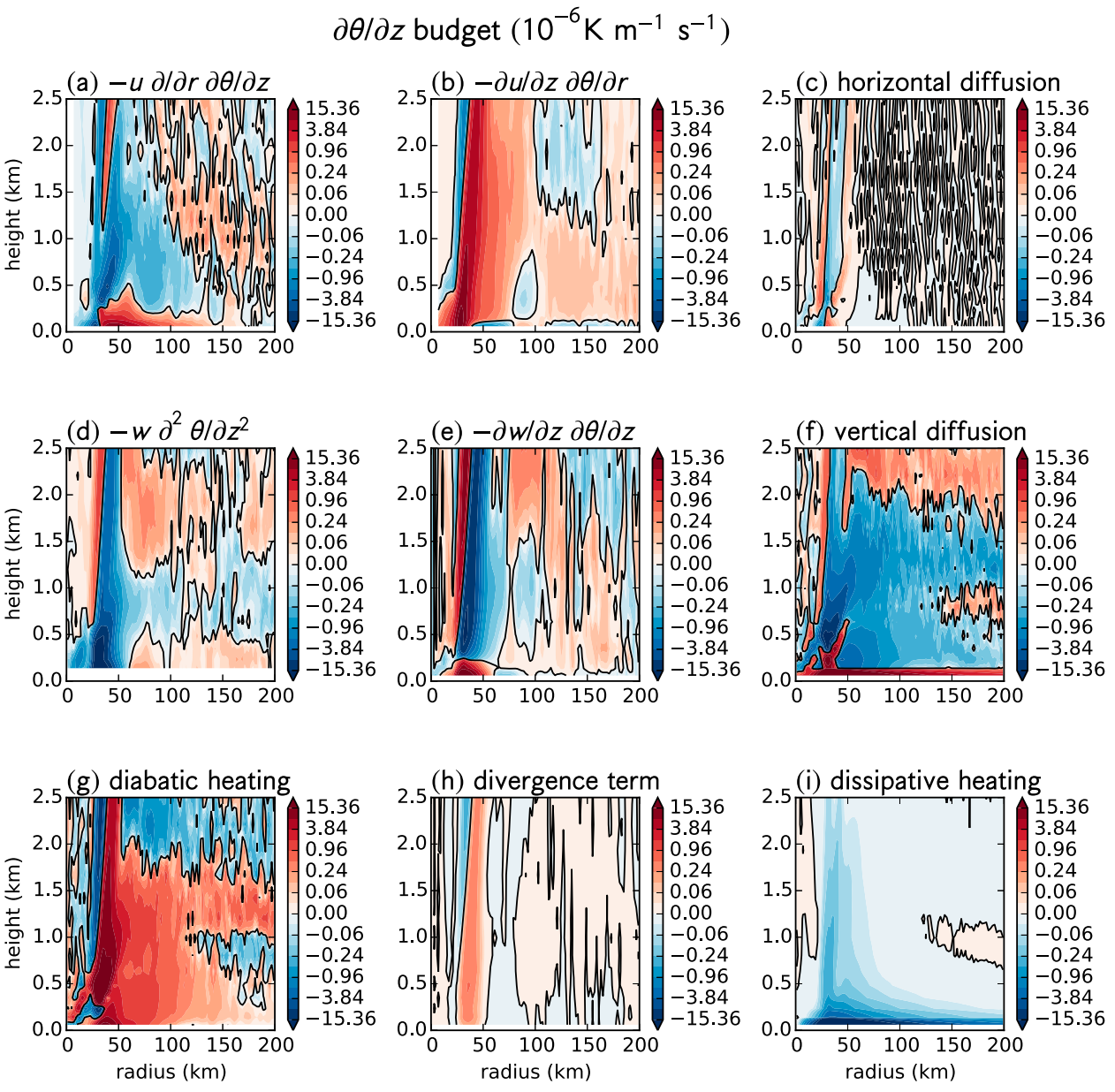

FIG. 9. As for Fig. 5, but for the run with dissipative heating on. (i) The vertical gradient of the dissipative heating rate.

documented by Zhang et al. (2011) appears to have two main causes. The first of these is diabatic processes due to the condensation of moist air and the evaporation of rainfall. These processes cause cooling near the surface, which diminishes with height and then changes sign to a warming. This gradient acts to make $\partial\theta/\partial z$ more positive. The second, but weaker, stabilizing influence is differential horizontal advection. The inflow is a maximum at about 100-m height, and the θ gradient is mostly directed inward in the boundary layer. Thus, cold-air advection is maximized at about this height, with a weaker cooling tendency above and below. This term thereby stabilizes much of the boundary layer, except close to the surface and in regions where the radial gradient is locally reversed.

Shpund et al. (2014) recently examined the thermal structure of the lowest 400 m of a tropical cyclone using a sea-spray transport model. Their results are broadly consistent with ours, albeit with some differences in the detail of the moist processes. Both studies agree that the sensible heat flux is downward in the upper part of the inflow layer and that this flux is important to the overall thermal structure. Both studies also agree on the importance of moist processes. However, while Shpund et al. (2014) show that moist processes, including the

formation of shallow cloud and drizzle, improve the match between the model and observations, their clouds can form at lower relative humidities than ours because they explicitly model sea spray and salt is hygroscopic. This regrowth of sea-spray drops as they are turbulently transported aloft was also shown by Kepert et al. (1999). On the other hand, their model domain is only 400 m deep, so they do not have deep convection dropping large amounts of rain into the subcloud layer and evaporatively cooling it as we do. They also do not include the effects of differential horizontal advection and dissipative heating.

The analysis of the tropical cyclone subcloud-layer budget by Betts and Simpson (1987), constrained by saturation point dynamics, similarly showed that cloud-base fluxes and droplet evaporation make substantial contributions to the thermodynamic budgets. The observational studies of Cione et al. (2000), Barnes and Bogner (2001), and Wroe and Barnes (2003) found a cooling in the lowest few hundred meters of the boundary layer outside of the RMW, which they attributed to cloud downdrafts and rainfall evaporation, and which is similar to that seen in our simulations.

Those authors and the results presented here agree that θ and the dry static stability are determined by processes that are quite different to those elsewhere in the atmospheric boundary layer. In particular, the conceptual model of the fair-weather daytime continental boundary layer does not apply in the tropical cyclone boundary layer because of the substantial diabatic contribution. Unfortunately, such models do tend to influence thinking; indeed, the conundrum of different definitions of the boundary layer top giving quite different results, as documented by Zhang et al. (2011) and others, rests on the assumption that the inversion height is a good diagnostic for boundary layer depth. Early experiments in atmospheric boundary layer research that led to these conceptual models were conducted in fair-weather, diurnally varying, horizontally homogeneous continental boundary layers. But we, like Dorothy and Toto, are not in Kansas anymore.

So, if the depth of the tropical cyclone boundary layer cannot be diagnosed in terms of the well-mixed (i.e., nearly constant θ) layer, how should it be detected? In the introduction, we quoted a typical textbook definition of the boundary layer, which included the words "the region most directly influenced by the exchange of momentum, heat and water vapour at the earth's surface" (Kaimal and Finnigan 1994, p. v). We do not see any reason for the definition in tropical cyclones to be different to that in the rest of the atmosphere. However, a definition such as the above can only be applied if we have a good knowledge of the turbulent momentum, heat, and moisture budgets; that is, substantially more knowledge than just vertical profiles of the mean wind, temperature, or moisture. While others have expressed the problem in terms of defining the boundary layer in terms of such data, we believe that it is more appropriate to instead seek a diagnostic or a proxy for the boundary layer top that can be derived from such data.

Latent heat release and absorption is among the largest terms in the θ budget and is largely responsible for the substantial dry static stability ($\partial\theta/\partial z \gg 0$) in the upper part of the inflow layer. Moist processes play a substantial role in the tropical cyclone boundary layer, so that θ is not determined mainly by surface fluxes and turbulent mixing, implying that it would be very difficult to diagnose boundary layer height from the θ profile.

Given the important role of moist processes, it is natural to consider whether a variable that is more nearly conserved under such processes than θ better delineates the boundary layer. Figure 10a shows a radius–height section of equivalent potential temperature θ_e in the run without dissipative heating (the other run is similar). Note that θ_e decreases with height to a midtropospheric minimum, which is at about 8 km in the eye and 3–3.5 km outside of the RMW. Within the RMW itself, the θ_e minimum is much lower, below 0.5 km, consistent with Barnes (2008, section 3a). Above these minima, θ_e increases toward the stratosphere at all radii.

Before we consider whether the θ_e field can provide a diagnostic for boundary layer height, we need to determine what that height is. Figures 10b and 10c shows the enthalpy and total momentum fluxes (shading), respectively. Both quantities decrease nearly monotonically from the surface, with the enthalpy flux changing sign near 3-km height outside the RMW and with the height of this sign change sloping steeply across the eyewall region. The black contours in these panels show these fluxes normalized by their surface value and are plotted at levels of ± 0.2. That is, outside of the eyewall, the enthalpy (momentum) flux has reduced to 20% of its surface value by 2–2.5 (1.5–2) km. At these radii, it therefore seems reasonable to say that the boundary layer height[2] is at 2 ± 0.5 km. Comparing this height to the θ_e section, there is no apparent feature in

[2] We are taking the height at which the turbulent fluxes become relatively small, rather than strictly zero, to indicate the top of the boundary layer because these fluxes are nonzero in much of the model domain, so requiring them to be strictly zero is meaningless. The boundary layer is, by definition, the region most directly influenced by exchanges at Earth's surface, so the surface fluxes provide an appropriate scale against which to measure "relatively small."

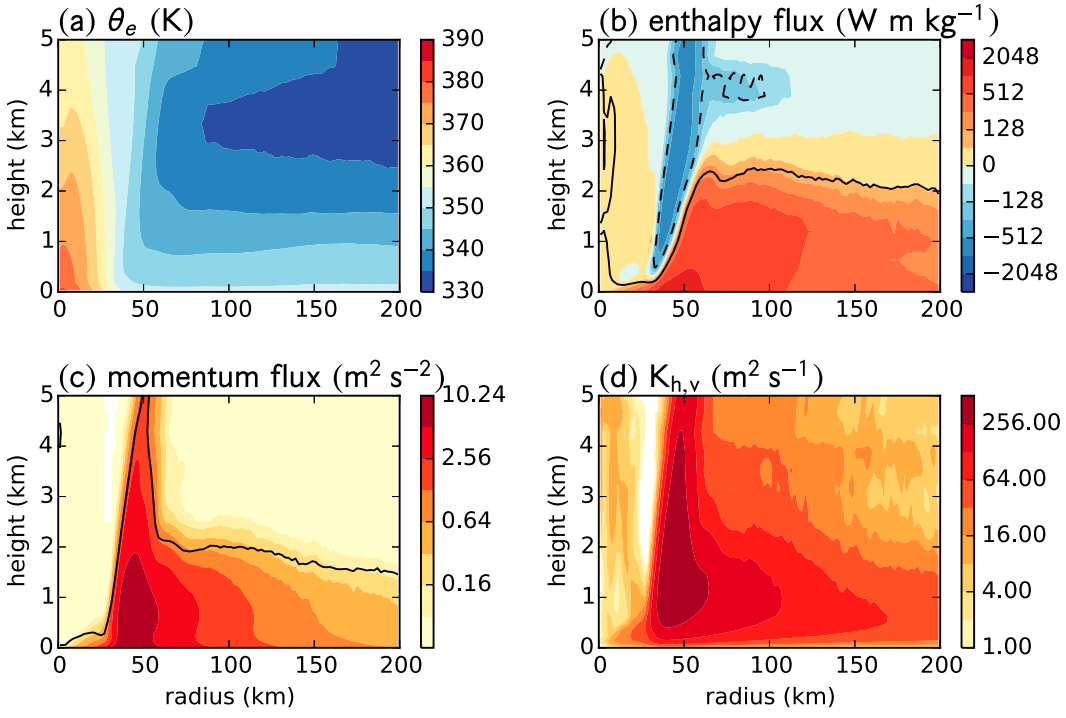

FIG. 10. Further radius–height plots from the model run without dissipative heating. (a) θ_e (contour interval 5 K). (b) Enthalpy flux (contours in geometric progression except for zero, at values of $\{0, \pm 64, \pm 128, \pm 256, \ldots, \pm 4096\} \times 10^{-5}$ K s^{-1}). (c) Total momentum flux (contours in geometric progression except for zero, at values of $\{0, 8, 16, 32, \ldots, 1024\} \times 10^{-2}$ m^2 s^{-2}). The black contours in (b) and (c) show the flux normalized by its surface value and at levels of 0.2 (solid) and −0.2 (dashed). (d) Turbulent vertical heat diffusivity, contours in geometric progressions at $1, 2, 4, \ldots, 512$ m^2 s^{-1}. Note that the height axis extends to 5 km here.

the θ_e field that might indicate the top of the boundary layer.

Within the eyewall region, the fluxes of enthalpy and momentum have a lobe that extends upward to much greater height. Consistency with the previous paragraph could require that we consider this to be part of the boundary layer and, indeed, the parameterized turbulence in this region (Fig. 10d) is largely generated by vertical shear of the horizontal wind. However, the shear in this region is due more to the cyclone warm core than to surface friction and the flow is close to gradient balance, so we conclude that this region should not be regarded as part of the boundary layer.

Alternatively, one could try to use a criterion based on the wind field. The most popular choice has been based on the depth of the inflow layer (e.g., Smith et al. 2009; Zhang et al. 2011). Arguments for this choice need to be carefully formulated because the argument that cross-isobar flow develops because surface friction retards the flow, destroying geostrophic (or gradient) balance and leading to a net force toward low pressure fails in the tropical cyclone boundary layer where the azimuthal flow in the upper part of the inflow layer in an axisymmetric cyclone is usually supergradient, and so the net force due to gradient imbalance there is directed outward toward high pressure (Kepert and Wang 2001). Kepert (2010a,b) presented simulations of an axisymmetric storm with a diagnostic tropical cyclone boundary layer model and two different turbulence parameterizations, in which the top of the inflow layer approximately coincided with the level at which the total stress reduced to 20% of its surface value, supporting the idea that the direct influence of the surface fluxes vanishes at or slightly above the top of the frictional inflow layer. Note, however, that those simulations lack the component of the secondary circulation due to diabatic heating. These results were extended here (Fig. 10) to show that the enthalpy flux similarly reduces to 20% of its surface value near the top of the inflow layer, except in the eyewall region. The top of the layer of strong inflow has the virtues of being easily detected from observation or model data and being easily understood. In particular, Smith et al.'s (2009) definition of the boundary layer includes "*strong* inflow near the sea surface" (p. 1322), although without specifying what they mean by strong, while Zhang et al. (2011) specify inflow greater than 10% of the peak inflow, which in their composite analysis corresponds to inflow

exceeding $2\,m\,s^{-1}$. One issue with such a definition is that part of the secondary circulation is induced by diabatic heating, and we should regard only the frictional inflow as indicating the boundary layer; for this reason Smith et al. (2009) and Zhang et al. (2011) exclude part of the inflow layer from their definition. Stern et al. (2015) have recently diagnosed the respective contributions of heating and friction to the secondary circulation and, in contrast to some earlier studies, obtained quite good quantitative agreement between the diagnosed total inflow in the lowest few kilometers and that in their model simulation. In their Fig. 14, the heating-induced inflow in the lowest 2 km ranges from 1 to $3\,m\,s^{-1}$, in good agreement with Zhang et al.'s (2011) criterion.

On the other hand, the turbulent momentum flux is a nonnegligible part of the dynamics of the outflow layer (Kepert and Wang 2001), suggesting that the boundary layer in the core of the tropical cyclone may be somewhat deeper than the frictional inflow layer.

A more serious problem with such definitions arises in moving storms, where the motion-induced asymmetry can lead to the inflow layer being much shallower or even absent in some regions, particularly in the left-rear quadrant of the storm. This behavior is seen in observations (Powell 1982) and idealized simulations (Kepert 2001; Kepert and Wang 2001) and was further discussed by Kepert (2010a,b). Clearly in such areas the absence of inflow does not imply a local absence of the boundary layer. A related problem with using the top of the inflow layer as a proxy in moving storms is that the depth scale of the motion-induced frictional asymmetry is significantly deeper than the frictional symmetric flow (Kepert 2001), so this criterion risks omitting a component of the flow that is directly due to surface friction.

A further possibility for detecting the boundary layer height is a criterion based on the Richardson number. However, we note that such criteria will inherit the difficulties that diabatic processes cause for proxies based on θ, unless a definition of Richardson number that accounts for the possibility of saturated air is used. We are not aware of any observational study in tropical cyclones that uses such a definition and expect that correcting for sensor wetting when dropsondes fall from cloudy to subcloud air might make such an analysis difficult.

Some boundary layer parameterizations operate by first detecting the boundary layer depth h and then using this height to define an analytical diffusivity function that is then used to calculate the fluxes. Examples of such parameterizations are the medium-range forecast (MRF) (Hong and Pan 1996) and Yonsei University (Hong et al. 2006) schemes. One possible issue with these parameterizations is that the results are sensitive to misdiagnosis of h, since the boundary layer mean diffusivity in them is proportional to h. Kepert (2012), in noting this issue, cautioned that users of such schemes should check that the diagnosed heights are reasonable. Recent studies with the Hurricane Weather Research and Forecasting system, which uses the MRF scheme, have found that better performance in hurricanes is obtained if the vertical diffusivity is reduced by a factor of 0.25 or 0.5 from that in the original version of that scheme (Gopalakrishnan et al. 2013; Zhang et al. 2015). We have shown why the thermal definition of the boundary layer top is different than the inflow layer in tropical cyclones, that the well-mixed layer is shallower than the inflow layer because of diabatic effects and horizontal advection (i.e., processes absent from simple conceptual models of the boundary layer), and that the turbulent fluxes are not approaching zero at this level. It may therefore be necessary to reexamine the validity of the algorithm for determining h in these parameterizations for tropical cyclone simulation.

5. Conclusions

In tropical cyclones, the vertical distribution of θ in the lowest 2 km is strongly influenced by moist processes—both latent heat release above cloud base and rainfall evaporation below. The change in radial θ advection with height due to wind shear in the frictionally induced inflow also modifies the structure away from one in which θ is constant with height, but the effects of this process are smaller than diabatic heating in our simulations. Hence, the ''well mixed'' layer (i.e., the layer of nearly constant θ) is shallower than the azimuthal-mean inflow layer as observed. As the top of this layer is determined by processes other than what are normally regarded as boundary layer dynamics, we recommend that it not be used as a diagnostic for the boundary layer height.

The near-surface inflow layer is a much better proxy for the boundary layer than the well-mixed layer, although the fact that some of the near-surface inflow is part of the heating-induced secondary circulation needs to be accounted for. Nevertheless, this proxy is problematic in moving storms, which can have regions of surface outflow, and in which the friction-induced motion asymmetry is known to be deeper than the symmetric friction-induced flow.

The observed near-surface layer in which the lapse rate is superadiabatic appears to be mainly due to heating from turbulent dissipation. Although differential radial advection also contributes to this layer, its contribution is smaller than that from dissipative heating

and a simulation with dissipative heating omitted produced a much less extensive and weaker superadiabatic region than observed.

In closing, we return to the notion of the boundary layer as the well-mixed layer. We discussed our misgivings regarding this term in the introduction and have shown that the depth of the layer of nearly constant θ in tropical cyclones is strongly influenced by diabatic effects and horizontal advection and is not a good proxy for the height at which the turbulent fluxes become small. Indeed, the part of the inflow layer above the constant-θ layer is turbulent, and previous studies have suggested that the turbulence there is largely shear generated, with the necessary shear ultimately due to surface friction within the storm. This layer possesses marked dry static stability but is, by any reasonable definition, well mixed. We therefore recommend against the use of this term in tropical cyclones as a synonym of ''nearly constant θ''.

Acknowledgments. George Bryan generously helped with CM1, particularly with calculating the θ budget. Jun Zhang kindly provided an updated version of the data in Zhang et al. (2011).

REFERENCES

Anthes, R. A., and S. Chang, 1978: Response of the hurricane boundary layer to changes of sea surface temperature in a numerical model. *J. Atmos. Sci.*, **35**, 1240–1255, doi:10.1175/1520-0469(1978)035<1240:ROTHBL>2.0.CO;2.

Barnes, G. M., 2008: Atypical thermodynamic profiles in hurricanes. *Mon. Wea. Rev.*, **136**, 631–643, doi:10.1175/2007MWR2033.1.

——, and M. D. Powell, 1995: Evolution of the inflow boundary layer of Hurricane Gilbert (1988). *Mon. Wea. Rev.*, **123**, 2348–2368, doi:10.1175/1520-0493(1995)123<2348:EOTIBL>2.0.CO;2.

——, and P. B. Bogner, 2001: Comments on ''Surface observations in the hurricane environment.'' *Mon. Wea. Rev.*, **129**, 1267–1269, doi:10.1175/1520-0493(2001)129<1267:COSOIT>2.0.CO;2.

Betts, A. K., and J. Simpson, 1987: Thermodynamic budget diagrams for the hurricane subcloud layer. *J. Atmos. Sci.*, **44**, 842–849, doi:10.1175/1520-0469(1987)044<0842:TBDFTH>2.0.CO;2.

Bister, M., and K. A. Emanuel, 1998: Dissipative heating and hurricane intensity. *Meteor. Atmos. Phys.*, **65**, 233–240, doi:10.1007/BF01030791.

Bryan, G. H., and J. M. Fritsch, 2002: A benchmark simulation for moist nonhydrostatic numerical models. *Mon. Wea. Rev.*, **130**, 2917–2928, doi:10.1175/1520-0493(2002)130<2917:ABSFMN>2.0.CO;2.

——, and R. Rotunno, 2009: The maximum intensity of tropical cyclones in axisymmetric numerical model simulations. *Mon. Wea. Rev.*, **137**, 1770–1789, doi:10.1175/2008MWR2709.1.

Chavas, D. R., and K. A. Emanuel, 2014: Equilibrium tropical cyclone size in an idealized state of axisymmetric radiative–convective equilibrium. *J. Atmos. Sci.*, **71**, 1663–1680, doi:10.1175/JAS-D-13-0155.1.

Cione, J. J., P. G. Black, and S. H. Houston, 2000: Surface observations in hurricane environment. *Mon. Wea. Rev.*, **128**, 1550–1561, doi:10.1175/1520-0493(2000)128<1550:SOITHE>2.0.CO;2.

Dunion, J. P., and C. S. Marron, 2008: A reexamination of the Jordan mean tropical sounding based on awareness of the Saharan air layer: Results from 2002. *J. Climate*, **21**, 5242–5253, doi:10.1175/2008JCLI1868.1.

Gopalakrishnan, S. G., F. D. Marks Jr., J. A. Zhang, X. Zhang, J.-W. Bao, and V. Tallapragada, 2013: A study of the impacts of vertical diffusion on the structure and intensity of the tropical cyclones using the high-resolution HWRF system. *J. Atmos. Sci.*, **70**, 524–541, doi:10.1175/JAS-D-11-0340.1.

Hakim, G. J., 2011: The mean state of axisymmetric hurricanes in statistical equilibrium. *J. Atmos. Sci.*, **68**, 1364–1376, doi:10.1175/2010JAS3644.1.

Hong, S.-Y., and H.-L. Pan, 1996: Nonlocal boundary layer vertical diffusion in a medium-range forecast model. *Mon. Wea. Rev.*, **124**, 2322–2339, doi:10.1175/1520-0493(1996)124<2322:NBLVDI>2.0.CO;2.

——, Y. Noh, and J. Dudhia, 2006: New vertical diffusion package with an explicit treatment of entrainment processes. *Mon. Wea. Rev.*, **134**, 2318–2341, doi:10.1175/MWR3199.1.

Kaimal, J. C., and J. J. Finnigan, 1994: *Atmospheric Boundary Layer Flows—Their Structure and Measurement*, Oxford University Press, 289 pp.

Kepert, J. D., 2001: The dynamics of boundary layer jets within the tropical cyclone core. Part I: Linear theory. *J. Atmos. Sci.*, **58**, 2469–2484, doi:10.1175/1520-0469(2001)058<2469:TDOBLJ>2.0.CO;2.

——, 2010a: Comparing slab and height-resolving models of the tropical cyclone boundary layer. Part I: Comparing the simulations. *Quart. J. Roy. Meteor. Soc.*, **136**, 1689–1699.

——, 2010b: Comparing slab and height-resolving models of the tropical cyclone boundary layer. Part II: Why the simulations differ. *Quart. J. Roy. Meteor. Soc.*, **136**, 1700–1711, doi:10.1002/qj.685.

——, 2012: Choosing a boundary layer parameterization for tropical cyclone modelling. *Mon. Wea. Rev.*, **140**, 1427–1445, doi:10.1175/MWR-D-11-00217.1.

——, 2013: How does the boundary layer contribute to eyewall replacement cycles in axisymmetric tropical cyclones? *J. Atmos. Sci.*, **70**, 2808–2830, doi:10.1175/JAS-D-13-046.1.

——, and Y. Wang, 2001: The dynamics of boundary layer jets within the tropical cyclone core. Part II: Nonlinear enhancement. *J. Atmos. Sci.*, **58**, 2485–2501, doi:10.1175/1520-0469(2001)058<2485:TDOBLJ>2.0.CO;2.

——, C. W. Fairall, and J.-W. Bao, 1999: Modelling the interaction between the atmospheric boundary layer and evaporating sea spray droplets. *Air-Sea Exchange: Physics, Chemistry and Dynamics*, G. L. Geernaert, Ed., Kluwer, 363–410.

Nolan, D. S., J. A. Zhang, and D. P. Stern, 2009a: Evaluation of planetary boundary layer parameterizations in tropical cyclones by comparison of in situ observations and high-resolution simulations of Hurricane Isabel (2003). Part I: Initialization, maximum winds, and the outer-core boundary layer. *Mon. Wea. Rev.*, **137**, 3651–3674, doi:10.1175/2009MWR2785.1.

——, D. P. Stern, and J. A. Zhang, 2009b: Evaluation of planetary boundary layer parameterizations in tropical cyclones by comparison of in situ observations and high-resolution simulations of Hurricane Isabel (2003). Part II: Inner-core boundary layer and eyewall structure. *Mon. Wea. Rev.*, **137**, 3675–3698, doi:10.1175/2009MWR2786.1.

Pauluis, O., and S. Garner, 2006: Sensitivity of radiative–convective equilibrium simulations to horizontal resolution. *J. Atmos. Sci.*, **63**, 1910–1923, doi:10.1175/JAS3705.1.

Powell, M. D., 1982: The transition of the Hurricane Frederic boundary-layer wind field from the open Gulf of Mexico to landfall. *Mon. Wea. Rev.*, **110**, 1912–1932, doi:10.1175/1520-0493(1982)110<1912:TTOTHF>2.0.CO;2.

——, P. J. Vickery, and T. A. Reinhold, 2003: Reduced drag coefficient for high wind speeds in tropical cyclones. *Nature*, **422**, 279–283, doi:10.1038/nature01481.

Ramsay, H. A., 2013: The effects of imposed stratospheric cooling on the maximum intensity of tropical cyclones in axisymmetric radiative–convective equilibrium. *J. Climate*, **26**, 9977–9985, doi:10.1175/JCLI-D-13-00195.1.

Rotunno, R., and K. A. Emanuel, 1987: An air–sea interaction theory for tropical cyclones. Part II: Evolutionary study using a nonhydrostatic axisymmetric numerical model. *J. Atmos. Sci.*, **44**, 542–561, doi:10.1175/1520-0469(1987)044<0542:AAITFT>2.0.CO;2.

Schneider, R. S., and G. M. Barnes, 2005: Low-level thermodynamic, kinematic, and reflectivity fields of Hurricane Bonnie (1998) at landfall. *Mon. Wea. Rev.*, **133**, 3243–3259, doi:10.1175/MWR3027.1.

Shpund, J., J. A. Zhang, M. Pinsky, and A. Khain, 2014: Microphysical structure of the marine boundary layer under strong wind and sea spray formation as seen from a 2D explicit microphysical model. Part III: Parameterization of height-dependent droplet size distribution. *J. Atmos. Sci.*, **71**, 1914–1934, doi:10.1175/JAS-D-12-0201.1.

Smith, R. K., and M. T. Montgomery, 2010: Hurricane boundary-layer theory. *Quart. J. Roy. Meteor. Soc.*, **136**, 1665–1670, doi:10.1002/qj.679.

——, ——, and V. S. Nguyen, 2009: Tropical cyclone spin-up revisited. *Quart. J. Roy. Meteor. Soc.*, **135**, 1321–1335, doi:10.1002/qj.428.

Stern, D. P., J. L. Vigh, D. S. Nolan, and F. Zhang, 2015: Revisiting the relationship between eyewall contraction and intensification. *J. Atmos. Sci.*, **72**, 1283–1306, doi:10.1175/JAS-D-14-0261.1.

Tory, K. J., J. D. Kepert, J. A. Sippel, and C. M. Nguyen, 2012: On the use of potential vorticity tendency equations for diagnosing atmospheric dynamics in numerical models. *J. Atmos. Sci.*, **69**, 942–960, doi:10.1175/JAS-D-10-05005.1.

Wroe, D. R., and G. M. Barnes, 2003: Inflow layer energetics of Hurricane Bonnie (1998) near landfall. *Mon. Wea. Rev.*, **131**, 1600–1612, doi:10.1175//2547.1.

Zhang, J. A., W. M. Drennan, P. G. Black, and J. R. French, 2009: Turbulence structure of the hurricane boundary layer between the outer rainbands. *J. Atmos. Sci.*, **66**, 2455–2467, doi:10.1175/2009JAS2954.1.

——, R. F. Rogers, D. S. Nolan, J. Marks, and D. Frank, 2011: On the characteristic height scales of the hurricane boundary layer. *Mon. Wea. Rev.*, **139**, 2523–2535, doi:10.1175/MWR-D-10-05017.1.

——, D. S. Nolan, R. F. Rogers, and V. Tallapragada, 2015: Evaluating the impact of improvements in the boundary layer parameterization on hurricane intensity and structure forecasts in HWRF. *Mon. Wea. Rev.*, **143**, 3136–3155, doi:10.1175/MWR-D-14-00339.1.